

1
2
3
4
5
6
7
8
9
10
11
12
13
14
15
16
17
18
19
20
21
22
23
24
25
26
27
28
29
30
31
32

**A new approach for modeling the Cenozoic oceanic
lithium isotope paleo-variations : the key role of climate**

Nathalie Vigier¹ & Yves Godderis²

¹Laboratoire d'Océanographie de Villefranche, CNRS, UPMC, 06230 Villefranche sur Mer, France. nathalie.vigier@obs-vlfr.fr (for correspondance)

²Géosciences Environnement Toulouse, CNRS, Université Paul Sabatier, 31400 Toulouse, France

32

33 **Abstract**

34

35 The marine record of the ocean lithium isotope composition may provide important
36 information constraining the factors that control continental weathering and how they have
37 varied in the past. However, the equations establishing the links between the continental flux
38 of Li to the ocean, its Li isotope composition and the ocean Li isotope composition are under-
39 constrained, and their resolution are related to significant uncertainties. In order to partially
40 reduce this uncertainty, we propose a new approach that couples the C and Li cycles, such
41 that our proposed reconstruction of the Cenozoic Li cycle is compatible with the required
42 stability of the exospheric carbon cycle on geological timescales. The results of this exercise
43 show, contrary to expectations, that the Cenozoic evolution of the Li isotope composition of
44 rivers does not have necessarily mimicked the oceanic $\delta^7\text{Li}$ rise. In contrast, variations in the
45 continental flux of Li to the ocean are demonstrated to play a major role in setting the ocean
46 $\delta^7\text{Li}$. We also provide evidence that Li storage in secondary phases is an important element of
47 the global Li cycle that cannot be neglected, in particular during the early Cenozoic. Our
48 modeling of the published foraminifera record highlight a close link between soil formation
49 rate and indexes recording the climate evolution during the Cenozoic, such as foraminifera
50 $\delta^{18}\text{O}$ and $p\text{CO}_2$ reconstructions. This leads us to propose that climate exerted a dominant
51 control on soil production rates during the last 70 Ma.

52

53

53 1. Introduction

54

55 Weathering (chemical erosion) of continental Ca-Mg rich silicates serves as a major sink of
56 atmospheric CO₂. However, determining how such weathering has evolved in the past, as a
57 function of climate or tectonic activity, remains a challenge. Filling this gap in our knowledge
58 is essential if we are to understand how global temperature is regulated on geological
59 timescales. The great potential of lithium isotopes to trace alteration processes has recently
60 been highlighted (see e.g. review in Burton & Vigier, 2011). Nevertheless, analytical
61 difficulties have limited their use as a marine paleoproxy. Misra & Froelich (2012, 2014)
62 determined the evolution of the lithium isotopic composition of bulk carbonates and
63 planktonic foraminifera over the past 68 Ma. These authors argue that this record reflects
64 ocean-wide variations, and that the 9‰ increase of the marine $\delta^7\text{Li}$ from the Paleocene to the
65 present (see figure 1), can be explained by an increase of river $\delta^7\text{Li}$ from 3‰ 60 Ma ago, to
66 23‰ at present. To account for such a rise in riverine $\delta^7\text{Li}$ Misra and Froelich (2012) invoke a
67 change of the alteration regime (from a congruent to a weathering- limited regime) and an
68 increase of clay formation (which fractionates Li isotopes) in mountainous - rapidly eroding -
69 areas. This assertion links the secular increase in the marine $\delta^7\text{Li}$ record to increasing tectonic
70 uplift and mountain building over the course of the Cenozoic. Under this interpretive
71 framework, continental weathering during the early Paleogene (\approx 60 Myrs ago) was
72 characterized principally by high dissolution rates of continental rocks and relatively low rates
73 of clay formation and transport. Such a weathering regime offers a mechanism for producing
74 low $\delta^7\text{Li}$ values in rivers, close to that of the continental crust, because dissolution is not
75 accompanied by significant Li isotope fractionation. Later in the Cenozoic, as tectonic activity
76 intensifies, incongruent weathering and clay formation is supposed to become more
77 significant, leading to a shift to larger riverine $\delta^7\text{Li}$.

78 However, several lines of evidence call this interpretation of the seawater record into
79 question, and in particular the notion that low $\delta^7\text{Li}$ values in rivers of the Cretaceous could be
80 sustained by predominately congruent weathering (Wanner et al., 2014). Indeed, a
81 congruency of the weathering process, that would correspond to small rates of clay formation
82 or soil production, at 60 Ma is not supported by the occurrence of thick weathering profiles
83 found at this period of time (e.g. Beauvais & Chardon, 2013; Tavlan et al., 2011; Meshram &
84 Randiv, 2011). In particular, the compilation of laterite formation by Beauvais and Chardon
85 (2013) shows that a major episode of laterite formation is centered on 55 Ma in West Africa,

86 at the time of the climatic optimum (Zachos et al., 2008) and when West Africa was located
87 in the warm and humid convergence zone. Laterite profiles have also been identified at high
88 latitudes during the same time interval. At least four spikes of lateritic formation are recorded
89 between 55 and 48 Ma the cause of it being identified as global warming (e.g. Retallack,
90 2010; 2014). A compilation of about 80 ODP or DSDP core sites indicate that the deep
91 seawater during the Paleocene exhibited low $\delta^{18}\text{O}$ values, with benthic foraminifera $\delta^{18}\text{O}$
92 values between 3 and 4 ‰ lower than at present (Zachos et al., 2001). This feature is
93 interpreted as much warmer climatic conditions, in agreement with recent reconstructions of
94 atmospheric $p\text{CO}_2$ at 60 Ma, ranging between 400 and 1000 ppmv (Beerling & Royer, 2011).
95 These conditions have favored the formation of thick weathering profiles, in particular of
96 lateritic regolith mantles rich in kaolinite and/or bauxite. These resistant phases are depleted
97 in major cations playing a key role in the carbon cycle (such as Ca and Mg), but they contain
98 significant amounts of Li. Our compilation of Li levels in kaolinite-rich samples (Table 1)
99 shows that they are - on average - similar to the Li content estimated for the continental crust
100 granites ($22\text{ppm}\pm 4\text{ppm}$, Teng et al., 2009). They may therefore have played a key role in the
101 continental Li cycle. Li-containing regoliths provide empirical evidence against the idea that
102 congruent weathering prevails during warm intervals of Earth history driving riverine $\delta^7\text{Li}$ to
103 values similar to average upper crust.

104 In this study, we propose a new modeling approach of the seawater record that consists in
105 coupling a simple mathematical description of the carbon and the lithium exospheric budget,
106 throughout the Cenozoic. The objective is not to produce an exhaustive study of the impact of
107 each parameter implied in the Li and the C cycle, but rather to show that for a given set of
108 parameters consistent with published estimations, there is an alternative solution that can
109 explain the Cenozoic $\delta^7\text{Li}$ oceanic variations.

110 Our model takes into account the changes in Li flux coming from the continents in response
111 to a balance between 1/ dissolution rates of continental rocks releasing Li in waters and 2/
112 temporary storage of Li into secondary phases formed in weathering profiles. Since lithium
113 isotopes fractionate during clay mineral accumulation (e.g. Huh et al., 2001; Kisakurek et al.,
114 2004; Rudnick et al., 2004), soil formation rate is expected to drive the Li isotope
115 composition of rivers. One illustration is that, at present, the mean $\delta^7\text{Li}$ value of the
116 continental runoff ($+23\text{‰}$; Huh et al., 1998) is much higher than the average $\delta^7\text{Li}$ value
117 estimated for the continental crust granites ($+2\pm 4\text{‰}$, Teng et al, 2009). Since Li isotopes do
118 not fractionate during dissolution, this difference is best explained by isotope fractionation

119 during the formation of secondary phases (Vigier et al., 2009; von Strandmann et al., 2010;
 120 Bouchez et al., 2013). Consequently, at present, at the world-wide scale, a significant part of
 121 the Li released by continental dissolution is stored in ⁶Li-rich soils, resulting in heavy
 122 signatures (⁷Li-rich) in rivers. Experimental investigations, as well as soil studies support
 123 these findings (e.g. Wimpenny et al., 2010; Vigier et al., 2008; Lemarchand et al, 2010).
 124 Thus, we explore how Li storage in soils at the global scale has affected the ocean $\delta^7\text{Li}$ value,
 125 as well as the potential of ocean $\delta^7\text{Li}$ to quantify the balance between physical denudation and
 126 chemical alteration and its variation throughout the Cenozoic.

127

128 **2. Model equations and basics**

129

130 *2.1. Seawater isotopic balance*

131

132 The two main sources of dissolved lithium to the ocean (oc) are river waters (riv) and high
 133 temperature hydrothermal fluids (hyd) (see Huh et al., 1998 and a detailed review in
 134 Tomascak, 2004 and in the supplementary material of Misra and Froelich, 2012). The main
 135 sink of oceanic lithium is its incorporation into authigenic phases, in particular marine clays
 136 which are the marine phases the most enriched in Li (Chan et al. , 2006). The seawater
 137 isotopic mass balance can thus be written as :

138

$$139 \quad M_{oc}^{Li} \cdot d\delta_{oc}/dt = F_{riv}(\delta_{riv}-\delta_{oc})+F_{hyd}(\delta_{hyd}-\delta_{oc})-F_{clay}(\delta_{oc}-\Delta_{oc}-\delta_{oc}) \quad (1)$$

140

141 where F is for the Li flux, and δ_{riv} δ_{oc} and δ_{hyd} are for the $\delta^7\text{Li}$ values of rivers, ocean and
 142 hydrothermal fluids respectively. Δ_{oc} represents the absolute value of the fractionation factor
 143 of the Li isotopes during marine secondary phase formation. In the literature, this factor is
 144 negative (preferential enrichment of the light ⁶Li isotope) and ranges between -10 and -25‰
 145 depending on the temperature at which authigenic phases are being formed (Chan et al, 1992;
 146 1993; Vigier et al., 2008).

147

148 The residence time of Li in the ocean is equal to 1 million years. Given that we are exploring
 149 the time evolution of its isotopic cycle over the whole Cenozoic (10^7 year timescale), we can
 150 assume steady-state for both the elemental (i.e. all the Li carried by rivers and released by
 151 hydrothermal activity into the ocean is removed through authigenic clay formation: $F_{riv} + F_{hyd}$

152 = F_{clay}) and isotopic Li cycles. The steady-state hypothesis is only valid for a timescale of
153 several million years (at least three times the Li residence time in the ocean).

154

155 Equation (1) becomes:

$$156 \quad F_{\text{riv}}(\delta_{\text{riv}} - \delta_{\text{oc}}) + F_{\text{hyd}}(\delta_{\text{hyd}} - \delta_{\text{oc}}) + F_{\text{riv}} \cdot \Delta_{\text{oc}} + F_{\text{hyd}} \cdot \Delta_{\text{oc}} = 0 \quad (2)$$

157

158 Consequently, we can solve the above equations for δ_{oc} :

$$159 \quad \delta_{\text{oc}} = (F_{\text{riv}}\delta_{\text{riv}} + F_{\text{hyd}}\delta_{\text{hyd}} + \Delta_{\text{oc}} \cdot (F_{\text{riv}} + F_{\text{hyd}})) / (F_{\text{riv}} + F_{\text{hyd}}) \quad (3)$$

160

161 where present-day published values for F_{riv} , F_{hyd} and Δ_{oc} are reported in Table 2. We consider
162 that the hydrothermal flux during the Cenozoic decreased slightly as a function of time,
163 following the curve described in Engebretson et al. (1992), based on variations of subduction
164 rates and mid-ocean ridge volume. This trend is currently used in numerical modeling of the
165 global carbon cycle and appears to be consistent with the Cenozoic climatic evolution
166 (Berner, 2004; Lefebvre et al., 2013).

167

168 Basically, equation 3 has two unknowns: $F_{\text{riv}}^{\text{Li}}$ and δ_{riv} . In previous studies (Hathorne and
169 James, 2006; Misra & Froelich, 2012), river $\delta^7\text{Li}$ has been interpreted as co-varying in a
170 straightforward way with the ocean $\delta^7\text{Li}$. However, one equation is not enough for two
171 independent unknowns. In contrast to the a priori expectation, the variation of the ocean $\delta^7\text{Li}$
172 composition during the Cenozoic may not reflect riverine $\delta^7\text{Li}$ variations in a straightforward
173 way. The reason for this is that it strongly depends on the continental Li flux too, which is
174 likely to have been strongly affected by variation in continental weathering rates during this
175 period of time. One purely theoretical example of the influence of the Li continental flux is
176 illustrated in Figure 2. This simulation shows that the 0-65Ma foraminifera $\delta^7\text{Li}$ record
177 (shown in figure 1) can still be fitted by imposing a constant river $\delta^7\text{Li}$ throughout the
178 Cenozoic, and using parameters values which are consistent with published data (Table 2).
179 We fixed the δ_{riv} ($\delta^7\text{Li}$ in rivers) to its present-day value (23‰). This is an extreme and
180 unlikely scenario because it does not account for change in the isotope fractionation due to
181 continental weathering. Indeed, the riverine $\delta^7\text{Li}$ is expected to vary as a function of the
182 relative importance of dissolution rate and clay formation rate (e.g. Bouchez et al., 2013).
183 However, this simulation shows that, by taking into account the Li ocean budget only, the
184 system of equations is under-constrained and it is not possible to calculate the temporal

185 variations of riverine $\delta^7\text{Li}$ without making assumptions about the link between $F_{\text{riv}}^{\text{Li}}$ and δ_{riv} .
186 It also shows that low seawater $\delta^7\text{Li}$, as highlighted by early Eocene foraminifera can be
187 compatible with a high $\delta^7\text{Li}$ value of the riverine flux. Our result shows therefore that low
188 $\delta^7\text{Li}$ in the ocean does not systematically imply low river $\delta^7\text{Li}$. The temporal variations of the
189 riverine Li flux also need to be established. In the following, we add constraints on this aspect
190 and the Li cycle, by coupling it to the carbon cycle.

191

192 2.2. Walker paleothermostat

193

194 The Walker paleothermostat (Walker et al., 1981) implies that, at the million year scale, the
195 consumption of carbon by silicate weathering ($F_{\text{riv}}^{\text{CO}_2}$) closely balances the release by
196 volcanic degassing (assumed to be proportional at first order to the seafloor spreading rate,
197 and hence to the hydrothermal activity) ($F_{\text{hyd}}^{\text{CO}_2}$), a condition absolutely needed to avoid
198 unrealistic atmospheric CO_2 fluctuations (Godderis & François, 1995; Kump & Arthur,
199 1997):

$$200 F_{\text{hyd}}^{\text{CO}_2} = F_{\text{riv}}^{\text{CO}_2} \quad (4)$$

201

202 During high temperature water-rock interactions, Li is known to be highly mobile, as
203 reflected by the large Li concentrations found in hydrothermal fluids located in mid-ocean
204 ridges (ppm level, Chan et al., 1994; Foustoukos et al., 2004; Mottl et al., 2011), and which
205 are ~ 3 orders of magnitudes greater than in river waters or seawater. Consequently, we
206 consider that the amounts of Li released by hydrothermal process is proportional to the carbon
207 flux released into the ocean:

208

$$209 F_{\text{hyd}}^{\text{CO}_2} = k_2 F_{\text{hyd}}^{\text{Li}} \quad (5)$$

210

211 with $k_2 = (\text{C/Li})$ of hydrothermal fluids (Table 2)

212 In contrast with hydrothermal conditions, Li is much less "mobile" on the continents,
213 as reflected by low Li contents in river waters (ppb level) while granites (the main source of
214 river Li) are enriched in Li compared to oceanic crust. Indeed, first, thermodynamic laws
215 indicate that dissolution rate is lower at lower temperature. Additionally, it is observed that
216 most of the Li carried by rivers to the ocean is mainly located in the particulate load ($>70\%$,
217 e.g. Millot et al., 2010), while the dissolved Li represents only a minor proportion. This is

218 consistent with the fact that Li can be significantly incorporated into the structure of
 219 secondary minerals, mainly clays. As a consequence, the flux of dissolved Li carried by rivers
 220 may not be proportional to the flux of CO₂ consumed during the leaching or dissolution of
 221 continental mineral phases. The relationship linking the flux of lithium carried by rivers and
 222 the flux of atmospheric CO₂ consumed by mineral dissolution becomes:

$$223$$

$$224 \quad F_{\text{riv}}^{\text{CO}_2} = 1/k_1 \cdot F_{\text{diss}}^{\text{Li}} = (F_{\text{riv}}^{\text{Li}} + F_{\text{sp}}^{\text{Li}}) / k_1 \quad (6)$$

225 $F_{\text{riv}}^{\text{Li}}$ and $F_{\text{sp}}^{\text{Li}}$ being the flux of lithium in river waters and in secondary phases respectively,
 226 and $F_{\text{diss}}^{\text{Li}}$ the flux of Li released into continental waters during the dissolution of continental
 227 rocks ($F_{\text{riv}}^{\text{Li}} = F_{\text{diss}}^{\text{Li}} - F_{\text{sp}}^{\text{Li}}$). k_1 is calculated assuming that dissolution of continental rocks
 228 release Li, Mg and Ca congruently. Also, we consider that 1 mol of atmospheric CO₂ is
 229 consumed by the dissolution of 1 mol of Mg+Ca present in continental rocks (accounting for
 230 the subsequent carbonate precipitation in the ocean) (Berner, 2004). Consequently, $k_1 = \text{Li}_{\text{UCC}}$
 231 / $(\text{Ca} + \text{Mg})_{\text{UCC}}$ (UCC being the Upper Continental Crust, Table 2).

232 If present-day conditions might reflect a recent disequilibrium due to the last glaciation
 233 (Vance et al., 2009), at the Cenozoic timescale, formation of thick weathering profiles with
 234 significant residence time (>0.5Ma) are likely to have impacted the Li cycle. We assume that
 235 most of secondary phases present in these profiles are largely depleted in cations, in particular
 236 in Ca and Mg, and therefore do not affect significantly the carbon budget. This is a first order
 237 approximation. Indeed, laterite in which the largely dominant clay phase is Mg-Ca free
 238 kaolinite, covers only 30% of the continental surfaces. However, owing to their thickness,
 239 they constitute about 85% of the global continental pedogenic cover (Nahon, 2003),
 240 supporting the above assumption.

241

242 Combining equation (4) (5) and (6) we obtain the following relationship:

$$243$$

$$244 \quad F_{\text{riv}}^{\text{Li}} = k_1 \cdot k_2 \cdot F_{\text{hyd}}^{\text{Li}} - F_{\text{sp}}^{\text{Li}} \quad (7)$$

245

246 where the flux of riverine Li is a function of both the hydrothermal flux and of the secondary
 247 phase formation rate on the continents.

248

249 *2.3. Riverine $\delta^7\text{Li}$*

251 All published studies indicate the existence of a strong isotope fractionation during the
 252 formation of secondary phases, such as clays or Fe oxides, always in favor of the light isotope
 253 (^6Li). At periods when the soil production and thickness increased in the past due to increase
 254 rate of secondary phase formation, we therefore expect that the $\delta^7\text{Li}$ of river waters increase,
 255 since more ^6Li is incorporated and stored into soils. In fact, the riverine $\delta^7\text{Li}$ is the result of
 256 the competition (e.g. Bouchez et al., 2013, Vigier et al., 2009) between the isotopically
 257 congruent dissolution of fresh bedrock, and the precipitation of secondary phases with an
 258 isotope fractionation Δ_{land} (Table 2), such that:

$$259 \quad 260 \quad F_{\text{riv}}^{\text{Li}} \delta_{\text{riv}} = \delta_{\text{UCC}} F_{\text{diss}}^{\text{Li}} - F_{\text{sp}}^{\text{Li}} (\delta_{\text{riv}} - \Delta_{\text{land}}) \quad (8)$$

261
 262 with δ_{UCC} being the average $\delta^7\text{Li}$ value estimated for the upper continental crust (Table 2).

263 Given that $F_{\text{diss}}^{\text{Li}} = F_{\text{riv}}^{\text{Li}} + F_{\text{sp}}^{\text{Li}}$, equation (8) becomes:

$$264 \quad 265 \quad \delta_{\text{riv}} = \delta_{\text{UCC}} + (F_{\text{sp}}^{\text{Li}} \Delta_{\text{land}}) / (F_{\text{riv}}^{\text{Li}} + F_{\text{sp}}^{\text{Li}}) \quad (9)$$

266
 267 This equation states that , if $F_{\text{sp}}^{\text{Li}} = 0$, then δ_{riv} equals δ_{UCC} . Otherwise, δ_{riv} is higher than δ_{UCC} .
 268 To date the published values of $\delta^7\text{Li}$ of most rivers (e.g. Huh et al., 1998, Millot et al., 2010;
 269 Kisakurek et al., 2004) are significantly greater than the $\delta^7\text{Li}$ estimated for UCC (2‰ , Teng
 270 et al. 2009), and thus are consistent with equation (9).

271 272 *2.4. Method for solving the model*

273
 274 We assume that the foraminifera $\delta^7\text{Li}$ reflect the ocean $\delta^7\text{Li}$, as assumed in Misra & Froelich
 275 (2012) and in Hathorne & James (2006). We consider that potential vital effects, responsible
 276 for changes of Li isotope fractionation during foraminifera growth may explain some
 277 observed rapid (<0.5Ma) changes of foraminifera Li isotope compositions, but we do not take
 278 into account these effects since the model aims at working at the multi million scale only. A
 279 moving average of the oceanic lithium isotopic data is calculated, with a window width of 5
 280 millions of years, since the isotopic steady-state is valid for a timescale of at least three times
 281 the Li residence time in the ocean (see figure 1). This data smoothing therefore ensures the
 282 validity of the steady-state hypothesis and removes all short term fluctuations potentially
 283 related to vital effects.

284

285 The equations describing the seawater isotopic budget (eq. 3), the paleothermostat (eq.
286 7), and the riverine isotopic budget (eq. 9) define a system of equations where the unknowns
287 are the riverine Li flux as a function of time (F_{riv}^{Li}), the storage flux of Li in soils (F_{sp}^{Li}), and
288 the riverine δ^7Li (δ_{riv}). It can be reduced to the following quadratic equation :

289

$$290 \quad A_1 (F_{riv}^{Li})^2 + (\delta_{oc} - \Delta_{oc} - \delta_{UCC} - \Delta_{land}) F_{riv}^{Li} - A_2 = 0. \quad (10)$$

291

292 Where A_1 and A_2 are equal to :

$$293 \quad A_1 = \Delta_{land} / (k_1 k_2 F_{Hyd}^{Li}) \quad (11)$$

$$294 \quad A_2 = F_{Hyd}^{Li} (\delta_{hyd} - \delta_{oc} + \Delta_{oc}) \quad (12)$$

295

296 The values for the various parameters used in the model are described in Table 2. As long as
297 the discriminant of eq. 10 is strictly positive, eq. 10 has two solutions for F_{riv}^{Li} . This means
298 that two radically different histories of F_{riv}^{Li} can both explain the rise of the Li isotopic
299 composition of seawater.

300

301 *2.5. Comparison with other modeling methods*

302

303 Recently, two modelings of the Cenozoic δ^7Li variations, different from Misra and Froelich
304 (2012, 2014) (section 1) have been proposed. Wanner et al. (2014) focused on a reactive
305 transport model in order to simulate the Li isotopic composition and content of continental
306 waters. Weathering reactions by sub-surface waters are simulated, considering a prescribed
307 thick regolith which already contains altered material (kaolinite and goethite), above a fresh
308 granite. Kinetic reactions based on transition state theory are used for calculating both the
309 dissolution and precipitation of mineral phases. River water chemistry is then considered to
310 be a simple dilution of these sub-surface waters having reacted with previously formed
311 profiles. Overall, the Wanner et al. (2014) model is designed to simulate finely the time
312 evolution of an already existing regolith profile and its impact on the riverine Li content and
313 isotopic composition. As acknowledged by the authors, the fit of the Cenozoic oceanic δ^7Li
314 curve cannot be computed as it would require the accurate knowledge of the Cenozoic climate
315 and runoff variations, to calculate the Li flux to the ocean as well as its isotopic composition.

316 The Wanner et al. (2014) model is a process-based model, but at this stage, it cannot account
317 for global budget.

318

319 Li and West (2014) proposed 12 different simulations for fitting the Cenozoic ocean $\delta^7\text{Li}$,
320 focusing their effort on potential variations of the oceanic Li sink and how this could have
321 affected the ocean $\delta^7\text{Li}$. They consider that the two major sinks of ocean Li are marine
322 authigenic alumino-silicate clays (during reverse weathering, at low temperature), and
323 removal into oceanic crust during its alteration by circulating fluids of moderate to high
324 temperatures. Both sinks are considered to be associated with a constant isotope fractionation
325 factor throughout the Cenozoic, but a varying proportion of both is considered to influence
326 the Li and $\delta^7\text{Li}$ removal flux. Then, a steady-state equation is applied to the ocean, identical to
327 the one used here, and different scenarii are tested to explore the impact of the mathematical
328 formulation of the oceanic Li sinks. Changes of river Li flux are assumed to be dependent on
329 the chemical weathering fluxes calculated by another model (Li and Elderfield, 2013), or
330 following the isotope balance method developed by Bouchez et al. (2013). Hydrothermal Li is
331 estimated from the reconstruction of spreading rate (Muller et al., 2008; Rowley, 2002). No
332 direct coupling with the carbon cycle is made.

333

334 At this stage, it is important to underline that, by coupling Li and C budgets, the solving of
335 our model equations does not require additional or independent assumptions for the
336 continental fluxes (dissolved and particulate) during the Cenozoic. Furthermore, our model is
337 based on budget equations only (for Li and C), and does not include any assumption on the
338 dependence of the fluxes on environmental conditions. The solid Earth degassing is extracted
339 from Egenbretson (1992). Although more recent reconstructions have been published, it has
340 been shown recently that the Egenbretson's curve is in good agreement with the Cenozoic
341 climate history (itself reconstructed using a coupled 3D climate-carbon model, see Lefebvre
342 et al., 2013). The precise Cenozoic history of the solid Earth degassing weakly influences our
343 results.

344

345

346

347

348

349

350 3. Results and discussion

351

352 3.1 Paleo-variations of continental weathering

353

354 Two solutions have thus been found for the Cenozoic (represented in figure 3A and 3B). The
355 first solution (figure 3A) implies an increase of the riverine $\delta^7\text{Li}$ over the Cenozoic,
356 associated to a decrease of riverine Li flux with time. This first solution is close to the
357 scenario described in details by Misra & Froelich (2012), arguing for an increasing
358 contribution of orogenesis on silicate dissolution, clay formation and CO_2 consumption
359 towards recent time. In this scenario, sequestration of lithium in clays increased from the past
360 towards the present day.

361 Our model results demonstrate that a second scenario can also explain the Cenozoic Li
362 isotope record. Indeed, figure 3B shows that the $\delta^7\text{Li}$ paleorecord mainly reflects an increase
363 of the riverine Li flux through the Cenozoic. As illustrated in figure 4, this increase is not due
364 to an increase in the dissolution rate of the silicate lithologies, but is mostly due to the
365 decrease of Li storage in secondary phases. Most Li-rich secondary phase are considered to be
366 formed within soil and lateritic profiles, and even if some have the time to be formed during
367 the river transport, this fraction is likely minor compared to the formation of thick soils and
368 kaolinite-rich laterite. Therefore, we consider that most of the Li storage during silicate
369 alteration occur in soils.

370 In order to test the robustness of our result, we performed two different simulations, using 1/
371 the whole set of equations (for both C and Li, see section 2), and 2/ an imposed variation of
372 δ_{riv} that is arbitrarily forced to increase linearly from 15‰ at 65 Ma to 23‰, its present day
373 value (in that case, only the Li budget is solved, not C). Both simulations lead to similar
374 trends, where Li_{soil} decrease as a function of time (see Figure 4). This strongly suggests the
375 robustness of the observed decrease, and also confirms that the Li isotope composition of
376 rivers plays only a minor role in the ocean isotopic variation. Overall, these results show that
377 soil Li storage was high from 65 to 50 Myr, and then decreased continuously until its
378 stabilization at about 20 Myrs ago (Figure 4).

379 In order to be more quantitative, check the consistency of these results and compare them to
380 other proxies, we estimated the corresponding soil formation rates, assuming a Li
381 concentration of 25ppm, which corresponds to an average soil Li concentration, including
382 data shown in Table 1. This is a first approximation because secondary phase formation rate
383 (calculated from Li data) may not strictly correspond to soil formation rate. Also, the

384 estimated average soil Li content may be associated with a large error, as there are currently
385 only few data. It may also have varied as a function of time, although this is not supported by
386 the relative narrow range of Li concentration of the most abundant clays. Nevertheless, this
387 assumption allows us to assess if the order of magnitude for the fluxes extracted from our
388 model makes sense. Also, a compilation of Li contents for the most abundant low-T
389 continental clays show that the average Li value is not so different from one type of clay to
390 another (Tardy et al., 1972; Table 1). During the Cenozoic, we thus estimate that soil
391 formation rate ranged from $2.2 \cdot 10^{19}$ kg/Ma to a present-day value of $1.3 \cdot 10^{19}$ kg/Ma, i.e.
392 $2.2 \cdot 10^{10}$ t/yr to $1.3 \cdot 10^{10}$ t/yr. For comparison, Syvitski et al. (2003) estimated a present-day
393 global physical denudation rate of $2 \cdot 10^{10}$ t/yr. The Syvitski denudation rate includes
394 secondary phases and fresh minerals but the most important here is that both orders of
395 magnitude are similar, and not totally at odd. Reconstitution of paleo-denudation rate during
396 the Cenozoic are controversial (e.g. Willenbring & von Blanckenburg, 2010), but given the
397 uncertainties typical of global scale estimations, it is worth noting that the calculated soil
398 formation falls quite close (less than an order of magnitude difference) to the independent
399 global denudation estimate, indicating that our calculations - based on C and Li cycles and
400 published values for corresponding parameters - make sense. Considering the uncertainties on
401 both estimations, a strict comparison between both numbers (physical and chemical erosion
402 rates) in order to determine if the erosion regime has globally remained close to steady-state
403 (where denudation rate and soil production rates are equal) during the Cenozoic does not
404 appear to be relevant yet.

405

406 **3.2 Assessing the role of climate**

407

408 Except for the last few Ma, the paleo-reconstruction of soil formation rate during the
409 Cenozoic is remarkably parallel to the $\delta^{18}\text{O}$ values measured in benthic foraminifera (Zachos
410 et al., 2001, see figure 5B). This strongly suggests a major role of climate on soil
411 development at the global scale. When the climate gets cooler, soil formation rates decrease.
412 A potential increase of weathering rates due to orogenesis and mountain building during the
413 Cenozoic is therefore not able to compensate the role of temperature. In the open debate
414 concerning the controls of continental chemical erosion rates at global scale over the
415 Cenozoic, Li isotopes yield good evidence of the predominance of climate over mechanical
416 erosion. Specifically the fact that soil formation rates predicted by the model parallel the

417 global benthic oxygen isotope record shows that the impact of orogenesis is not strong
418 enough to counter-balance the impact of temperature decrease.

419 More closely inspecting the comparison between soil formation rate, $\delta^{18}\text{O}$ and $p\text{CO}_2$ paleo-
420 variations reveals four remarkable features:

421 1/ High soil formation rates during the Paleocene and Early Eocene, coincides with
422 high $p\text{CO}_2$ estimations (Beerling and Royer, 2011) as well as low foraminifera $\delta^{18}\text{O}$ values.
423 This strongly suggests that weathering rates were high because of climatic conditions
424 favoring both dissolution of silicate rocks and formation of secondary minerals and laterites.
425 In order to explain the high riverine $\delta^7\text{Li}$ values associated to low Li flux at this period of time
426 (see Figure 3B), our budget equations require a massive transformation of fresh rocks into
427 regolith. An important soil production also requires important weathering rates, consistent
428 with high estimated atmospheric $p\text{CO}_2$ levels. This intense weathering leads to worldwide
429 production of thick lateritic profiles, which is evidenced in many parts of the world (e.g.
430 Beauvais and Chardon, 2013; Retallack, 2010; Tabor and Yapp, 2005; Robert and Kennett,
431 1992).

432 2/A sharp decrease of soil formation rate coeval with a sharp increase in foraminifera
433 $\delta^{18}\text{O}$ during the Eocene until the beginning of the Oligocene. This co-variation suggests a
434 predominant role of climate cooling on continental soil production. However, during this
435 period of time, we cannot exclude a global thinning of soils by mountain building and
436 orogenesis. Steeper slopes, higher relief, and increasing impact of landslide contribute
437 significantly to reduce the world average soil thickness.

438 3/A stabilization of the weathering rates between 30 and 10Ma, which matches the
439 plateaus exhibited by $p\text{CO}_2$ (not shown here, but see Beerling and Royer, 2011) and $\delta^{18}\text{O}$
440 proxies.

441 4/ A decoupling between soil formation rate, benthic foraminifera $\delta^{18}\text{O}$ and physical
442 denudation rate during the Quaternary period. Indeed, both soil formation rates and $p\text{CO}_2$
443 estimates remain globally stable during this period. However, foraminifera $\delta^{18}\text{O}$ and
444 denudation rates (e.g. Hay et al., 1988) show significant variations, consistent with the
445 development of a cool climate and glaciations. Reconstructions of $^{10}\text{Be}/^9\text{Be}$ in the ocean also
446 suggest a constancy of the continental weathering rates for the last 5-10 Ma and have
447 questioned the relationship between physical and chemical erosion rates (Willenbring and von
448 Blanckenburg, 2010). Our results suggest that the recent climatic variations were not strong
449 enough to affect the Li cycle, as evidenced by constant foraminifera $\delta^7\text{Li}$ value during the last

450 5Ma. The other possibility is that the present-day residence time of Li in the ocean is
451 underestimated and the chemical - and potentially physical - disturbances related to
452 Quaternary glaciations did not have time yet to significant affect its oceanic budget.

453

454 **3.3 Open questions**

455

456 Our result for the Paleocene/Eocene boundary differs from previous modelings in two
457 ways: first, the low ocean $\delta^7\text{Li}$ values at the P/E boundary may not necessarily require low
458 riverine $\delta^7\text{Li}$ values, as previously considered in Wanner et al., (2014), in Misra and Froelich
459 (2012) and in Li and West (2014). Secondly, at a period of time where weathering profiles are
460 abundant and thick, Wanner et al. (2014) reactive transport model shows that low riverine
461 $\delta^7\text{Li}$ such as observed at the Paleocene-Eocene boundary can be explained by predominant
462 dissolution of previously formed secondary phases occurring in pre-formed thick regoliths
463 (rich in kaolinite and goethite) (see section 2.5). The inverse relationship between regolith
464 thickness and riverine $\delta^7\text{Li}$ arises from a longer residence time of water in contact with
465 depleted secondary phases during periods characterized by weak tectonic activity and low
466 physical erosion rates. In contrast, our model, which is based on budget equations only,
467 implies that the formation of secondary phases from fresh bedrock produce an increase of
468 river $\delta^7\text{Li}$, because ^6Li is preferentially stored in regolith in formation.

469 Future studies should merge both methods such that transformation of the fresh
470 bedrock into regolith and the building of thick weathering profiles can be accounted for, as
471 well as the reactivity of the regolith itself.

472

473 The amount of published Li concentrations in various types of clay is still too limited
474 to estimate precisely the Li mobility at the continental scale. At present, river particles carry
475 more than 80% of the river total Li flux (calculation based on discharge and fluxes published
476 by Gaillardet et al., 1999 and published average Li concentration for river water and
477 suspended particles, Huh et al., 1998; 2001; Kisakurek et al., 2005; Millot et al., 2010;
478 Dellinger et al., 2014). At 55Ma, the Li storage in soils is pretty close to 100% (following
479 solution B). This corresponds precisely to the longest and one of the most intense weathering
480 events of the Cenozoic in western Africa (Beauvais and Chardon, 2013), and probably
481 elsewhere in the world (Rettalack, 2010). Conversely, case A predicts that only 20% of Li is
482 retained during this event. Constraining more precisely the role of Li-rich kaolinite formation

483 in soils and laterites would certainly add precious information to the debate. A recent study of
484 Hawaiian basaltic soil chronosequence (Ryu et al., 2014) shows that Li is retained at 100% in
485 soil layers rich in kaolinite, which further supports their critical role, but more investigation at
486 larger scale is now required.

487

488 In our modeling, the hydrothermal carbon flux is assumed to be strictly compensated
489 by continental silicate weathering. The potential role of other sources/sinks of carbon has
490 been neglected at this stage, in particular the influence of metamorphism and of organic
491 matter burial. Indeed, disequilibria in the organic carbon subcycle may alter the
492 proportionality between the total CO₂ consumption by continental silicate weathering and the
493 CO₂ released hydrothermal activity. In the case of the strontium cycle for instance, it is well
494 known that such additional processes may produce non negligible fluctuations of the oceanic
495 isotopic composition (Godd ris and Fran ois, 1995). In the case of the Li cycle, these
496 processes are not expected to influence directly the Li fluxes and their isotope signatures.
497 However, change of carbon fluxes can potentially produce alteration of the Li isotopic
498 composition of the ocean. This is an important field for future investigations. The objective
499 here was to decipher the first order control factors on the time evolution of the Li cycle. The
500 calculated scenarii must be seen as a background history, neglecting at this stage processes
501 that could modulate the model output around the proposed long-term averaged evolution.

502

503 Although our model depends on the Li content of the continental silicate rock being
504 altered, there is no constraint on how these contents may fluctuate globally during the
505 Cenozoic. Determining how each rock type (basalt, granite, shales) contributes to the global
506 weathering flux, according to change in climate, vegetation and tectonic settings is beyond the
507 capability of our simple model. This aspect is currently explored with coupled 3D-
508 climate/biogeochemical models (Taylor et al., 2012; Lefebvre et al., 2013), showing for
509 example that the position of India relative to the tropical belt strongly controls the alteration
510 of the Deccan Traps lava flows. Exploring the impact of this on the lithium cycle is a task for
511 the future.

512

513

514

515

516

517 **4. Conclusion**

518

519 We provide a new approach for modeling the seawater $\delta^7\text{Li}$ record, preserved in marine
520 foraminifera and carbonate records (Misra and Froelich, 2012). The Li cycle includes several
521 fluxes of importance for the carbon cycle (and hence for the climatic evolution), including
522 continental weathering and hydrothermal water-rock interactions. For this reason, we have
523 combined the C and the Li cycles, so that our proposed reconstruction of the Cenozoic Li
524 cycle is compatible with the required stability of the exospheric carbon cycle at the geological
525 timescale (Walker et al., 1981). Results are consistent with the current knowledge of the
526 behavior of Li isotopes during continental weathering: 1/ in terms of isotope fractionation
527 during dissolution and clay formation 2/in term of present-day river flux and river $\delta^7\text{Li}$.

528 In order to fit the paleovariation of the ocean $\delta^7\text{Li}$ through out the Cenozoic, the model
529 required significant Li to be stored on the continents during the Paleocene and Eocene, likely
530 in secondary phases which are Li-rich, such as phyllosilicates and oxides. Then this storage
531 flux globally decreases towards the present day, while the export to the ocean by weathering
532 increases. This storage follows indexes recording the climate evolution during the Cenozoic,
533 such as foraminifera $\delta^{18}\text{O}$ and $p\text{CO}_2$ reconstructions. This leads us to propose that climate
534 exerted a dominant control on soil production rates during the last 70 Ma.

535

References

- 535
536
537
538 Beauvais, A., and D. Chardon Modes, tempo, and spatial variability of Cenozoic cratonic
539 denudation: The West African example, *Geochem. Geophys. Geosyst.*, 14, 1590–1608,
540 doi:10.1002/ggge.20093, 2013
- 541 Beerling D. J., Royer D.R., Convergent Cenozoic CO₂ history, *Nature Geoscience* 4, 418-
542 420, doi:10.1038/ngeo1186, 2011
- 543 Berner, R.A., *The Phanerozoic carbon cycle: CO₂ and O₂*, Oxford University Press. pp160,
544 2004
- 545 Bouchez J., Von Blanckenburg F. and Schuessler J. A., Modeling novel stable isotope ratios
546 in the weathering zone, *Am. J. Science* 313, 267–308, 2013, DOI 10.2475/04.2013.01, 2013
- 547 Burton K.W. & Vigier N. Lithium isotopes as tracers in marine and terrestrial
548 environments. *Handbook of Environmental Isotope Geochemistry*, 41-61, 2011
- 549 Chan, L.-H., W. P. Leeman, and T. Plank, Lithium isotopic composition of marine
550 sediments, *Geochem. Geophys. Geosyst.*, 7, Q06005, doi:10.1029/2005GC001202, 2006
- 551 Chan L.-H., Edmond J.M., Thompson G. and Gillis K., Lithium isotopic composition of
552 submarine basalts: implications for the lithium cycle to the ocean. *Earth Planet. Sci. Lett.* 108,
553 151–160, 1992
- 554 Chan L.-H., Edmond J. M. and Thompson G., A lithium isotope study of hot springs and
555 metabasalts from mid ocean ridge hydrothermal systems. *J. Geophys. Res.* 98, 9653–9659,
556 1993
- 557 Chan L.-H., Gieskes J. M., You C-F and Edmond J. M., Lithium isotope geochemistry of
558 sediments and hydrothermal fluids of the Guaymas Basin, Gulf of California, ~, *Geochim.*
559 *Cosmochim. Acta* 58, 4443-4454, 1994
- 560 Dellinger M., Gaillardet J., Bouchez J., Calmels D., Galy V., Hilton R. G., Louvat P.,
561 France-Lanord C., Lithium isotopes in large rivers reveal the cannibalistic nature of modern
562 continental weathering and erosion, *Earth Planet. Sci. Lett.* 401, 359-372, 2014
- 563 Engebretson, D.C., Kelley, K.P., Cashman H.J., Richard M.A., 180 million years of
564 subduction, *GSA Today* 2, 93-100, 1992
- 565 Godderis Y., Francois L.M., The Cenozoic evolution of the strontium and carbon cycles:
566 relative importance of continental erosion and mantle exchanges, *Chem. Geol.* 126 169-190,
567 1995
- 568 Foustoukos, D.I., James, R.H., Berndt, M.E., Seyfried, W.E. Jr., Lithium isotopic

569 systematic of hydrothermal vent fluids at the Main Endeavour Field, Northern Juan de Fuca
570 Ridge. *Chem. Geol.* 212, 17-26, 2004

571 Hathorne, E. C., James, R. H., Temporal record of lithium in seawater: A tracer for silicate
572 weathering? *Earth Planet. Sci. Lett.* 246, 393–406, 2006

573 Hay, W. W., Sloan, J. L. I. & Wold, C. N. The mass/age distribution of sediments on the
574 ocean floor and the global rate of loss of sediment. *J. Geophys. Res.* 93, 14933–14940, 1988

575 Huh, Y., Chan, L.-H., Edmond, J. M., Lithium isotopes as a probe of weathering processes:
576 Orinoco River. *Earth Planet. Sci. Lett.* 194, 189–199, 2001

577 Huh Y., Chan L-H, Zhang L., Edmond J. M., Lithium and its isotopes in major world
578 rivers: Implications for weathering and the oceanic budget, *Geochim. Cosmochim. Acta* 62,
579 2039–2051, 1998

580 Kisakurek, B., Widdowson, M., James, R. H., 2004. Behaviour of Li isotopes during
581 continental weathering: the Bidar laterite profile, India. *Chem. Geol.* 212, 27–44

582 Kisakürek, B., James, R.H., Harris, N.B.W., Li and $\delta^7\text{Li}$ in Himalayan rivers: Proxies for
583 silicate weathering? *Earth Planet. Sci. Lett.* 237, 387-401., 2005

584 Kump, L.R. and Arthur, M.A., Global chemical erosion during the Cenozoic:
585 Weatherability balances the budgets. In: Ruddiman, W., ed., *Tectonics Uplift and Climate*
586 *Change*, Plenum Press., N.Y., 399-426, 1997.

587 Lear, C. H., Elderfield, H. and Wilson, P. A., A Cenozoic seawater Sr/Ca record from
588 benthic foraminiferal calcite and its application in determining global weathering
589 fluxes. *Earth and Planetary Science Letters* 208(1-2), 69-84, 2003

590 Lefebvre V, Donnadiou Y, Godd ris Y, Fluteau F, Hubert-Th ou L, Was the Antarctic
591 glaciation delayed by a high degassing rate during the early Cenozoic?, *Earth Planet. Sci.*
592 *Lett.* 371, 203-211, 2013

593 Lemarchand E., Chabaux F., Vigier N., Millot R., Pierret M-C, Lithium isotope
594 systematics in a forested granitic catchment (Strengbach, Vosges Mountains, France),
595 *Geochim. Cosmochim. Acta* 74, 4612–4628, 2010

596 Li G. and Elderfield H., Evolution of carbon cycle over the past 100 million years,
597 *Geochim. Cosmochim. Acta* 103, 11–25, 2013

598 Li G-J. and West A.J., Evolution of Cenozoic seawater lithium isotopes: coupling of global
599 denudation regime and shifting seawater sinks. *Earth and Planetary Science Letters* 401: 284-
600 293. doi: 10.1016/j.epsl.2014.06.011, 2014

601 Meshram R.R., Randive K.R., Geochemical study of laterites of the Jamnagar district,
602 Gujarat, India: Implications on parent rock, mineralogy and tectonics, *J. Asian Earth Sci.* 42,
603 1271-1287, <http://dx.doi.org/10.1016/j.jseaes.2011.07.014>, 2011

604 Millot R, Vigier N, Gaillardet J, Behaviour of lithium and its isotopes during weathering in
605 the Mackenzie Basin, Canada. *Geochim. Cosmochim. Acta* 74, 3897-3912, 2010

606 Misra, S. & Froelich, P. N., Lithium Isotope History of Cenozoic Seawater: Changes in
607 Silicate Weathering and Reverse Weathering, *Science* 335, 818-823, 2012

608 Froelich F. and Misra S. Was the Late Paleocene-Early Eocene Hot Because Earth Was
609 Flat? An Ocean Lithium Isotope View of Mountain Building, Continental Weathering,
610 Carbon Dioxide, and Earth's Cenozoic Climate, *Oceanography* 27 (1), 36-49, 2014

611 Mottl, M.J., Seewald, J.S., Wheat, C.J., Tivey, M.K., Michael P.J., Proskurowski, G.,
612 McCollom, T.M., Reeves, E., Sharkey, J., You, C.F., Chan, L.H., Pichler T., Chemistry of hot
613 springs along the Eastern Lau Spreading Center, *Geochim. Cosmochim. Acta* 75, 1013-1038,
614 2011.

615 Muller R.D., Sdrolias M., Gaina C., Roest W., Age, spreading rates, and spreading
616 asymmetry of the world's ocean crust. *Geochem. Geophys., Geosys.*, 9, doi:
617 10.1029/2007GC001743, 2008

618 Nahon D., Alterations dans la zone tropicale. Signification à travers les mécanismes
619 anciens et/ou encore actuels. *C.R. Geoscience*, 335, 1109-1119, 2003

620 Retallack G.J.. Laterization and bauxitization events. *Economic Geology*, 105, 655-667,
621 2010

622 Retallack G.J., Cool-climate or warm-spike lateritic bauxites at high latitudes ? *J. Geol.*,
623 116,558-570, 2014

624 Robert C., Kennett J.P., Paleocene and Eocene kaolinite distribution in the South Atlantic
625 and Southern Ocean: Antarctic climatic and paleoceanographic implications. *Mar. Geol.*, 103,
626 99-101, 1992

627 Rowley D.B., Rate of plate creation and destruction: 180 Ma to present. *GSA Bull.*, 114,
628 927-933, 2002

629 Rudnick R. L., Tomascak P. B., Njoa H. B., Gardner L. R., Extreme lithium isotopic
630 fractionation during continental weathering revealed in saprolites from South Carolina, *Chem.*
631 *Geol.* 212, 45– 57, 2004

632 Ryu J-S, Vigier N, Lee S-W, Chadwick O, Variation of lithium isotope geochemistry
633 during basalt weathering and secondary mineral transformations. *Geochim. Cosmochim. Acta*
634 145: 103-115, 2014

635 von Strandmann PAEP, Burton KW, James RH, van Calsteren P, Gislason SR, Assessing
636 the role of climate on uranium and lithium isotope behaviour in rivers draining a basaltic
637 terrain, *Chem. Geol.* 270, 227-239, 2010

638 Syvitski J.P.M., S.D. Peckham, Hilberman R., Mulder T., Predicting the terrestrial flux of
639 sediment to the global ocean: a planetary perspective, *Sedimentary Geology* 162 5–24, 2003

640 Tabor N.J., Yapp C.J., Coexisting goethite and gibbsite from a high-paleolatitude (55°N)
641 late Paleocene laterite; concentration and $^{13}\text{C}/^{12}\text{C}$ ratios of occluded CO_2 and associated
642 organic matter/ *Geochim. Cosmochim. Acta*, 69, 5495-5510, 2005

643 Taylor L.L., Banwart S.A., Valdes P.J., Leake J.R., Beerling D.J., Evaluating the effects of
644 terrestrial ecosystems, climate and carbon dioxide on weathering over geological time: a
645 global scale process-based approach. *Phil. Trans. R. Soc. B*, 367, 565-582, 2012

646 Tardy Y., Krempf G. et Trauth N, Le lithium dans les minéraux argileux des ciments et
647 des sols, *Cosmochim. Acta* 36, 397-412, 1972.

648 Tavlan M., Thorne R. & Herrington R. J., Uplift and lateritization history of the Caldag
649 ophiolite in the context of Neo-Tethyan ophiolite obduction and uplift: implications for the
650 Cenozoic weathering history of western Anatolia, *J. Geol. Soc. London* 168, 927–940. 2011,

651 Teng F-Z, Rudnick R. L., McDonough W. F., Wu F.Y., Lithium isotopic systematics of A-
652 type granites and their mafic enclaves: Further constraints on the Li isotopic composition of
653 the continental crust, *Chem. Geol.* 262, 370–379, 2009

654 Tomascak, P. B., Developments in the understanding and application of lithium isotopes in
655 the Earth and Planetary Sciences. *Rev. Mineral. Geochem.* 55, 153–195, 2004

656 Vance, D. Teagle D.A.H. and Foster G.L. Variable Quaternary chemical weathering rates
657 and imbalances in marine geochemical budgets, *Nature*, 458, 493-496, 2009

658 Vigier, N., Gislason, S. R., Burton, K. W., Millot, R., Mokadem, F., The relationship
659 between riverine lithium isotope composition and silicate weathering rates in Iceland. *Earth
660 Planet. Sci. Lett.* 287, 434-441, 2009

661 Vigier N, Decarreau A, Millot R, Carignan J, Petit S, France-Lanord C, Quantifying Li
662 isotope fractionation during smectite formation and implications for the Li cycle. *Geochim.
663 Cosmochim. Acta* 72, 780-792, 2008

664 Wanner C., Sonnenthal E. L., Liu X.-M, Seawater $\delta^7\text{Li}$: a direct proxy for global CO_2
665 consumption by continental silicate weathering? *Chem. Geol.* 381, 154-167, 2014

666 Wimpenny J., Gislason S. R, James R. H, Gannoun A., Von Strandmann P., Burton K.W,
667 The behaviour of Li and Mg isotopes during primary phase dissolution and secondary mineral
668 formation in basalt, *Geochim. Cosmochim. Acta* 74 (18), 5259-5279, 2010

669 Walker J.C.G., Haysand P.B., and Kasting J.F. A negative feedback mechanism for the
670 long-term stabilization of Earth's surface temperature. *J. Geophys. Res.*, 86(C10) : 9776–
671 9782, 1981.

672 Willenbring J. K. & von Blanckenburg F., Long-term stability of global erosion rates and
673 weathering during late-Cenozoic cooling, *Nature* 465, 211-214, 2010

674 Zachos, J. C., Shackleton, N. J., Revenaugh, J. S., Pälike, H., and Flower, B. P., Climate
675 response to orbital forcing across the Oligocene-Miocene boundary, *Science* 292, 274-
676 277, 2001

677 Zachos J.C., Dickens G.R., Zeebe R.E., An early Cenozoic perspective on greenhouse
678 warming and carbon-cycle dynamics, *Nature*, 451, 279-283, 2008

679

680

680

681 **Table 1:** Li concentrations measured in kaolinite (Tardy et al., 1972). These clays contain
682 0.2% MgO (Tardy et al., 1972). On average, the Li level for kaolinite is estimated to be 23
683 ppm. For comparison, average Li content for smectite is found to be 27 ppm (Tardy et al.,
684 1972) and 22 ppm for granites (Teng et al., 2009).

<i>location</i>	<i>Li (ppm)</i>	<i>Reference</i>
Ivory Coast	30	Tardy et al. (1972)
	23	Tardy et al. (1972)
	53	Tardy et al. (1972)
	70	Tardy et al. (1972)
	22	Tardy et al. (1972)
	26	Tardy et al. (1972)
	4	Tardy et al. (1972)
	7	Tardy et al. (1972)
	7	Tardy et al. (1972)
	8	Tardy et al. (1972)
	32	Tardy et al. (1972)
	37	Tardy et al. (1972)
	5	Tardy et al. (1972)
	35	Tardy et al. (1972)
USA	20	Rudnick et al. 2004
Seine basin (France)	42	t.s.
Brazilian Amazon Basin	6.3	t.s
	5.3	t.s
	11.5	t.s
	11.8	t.s
Average Kaolinite	23	

685

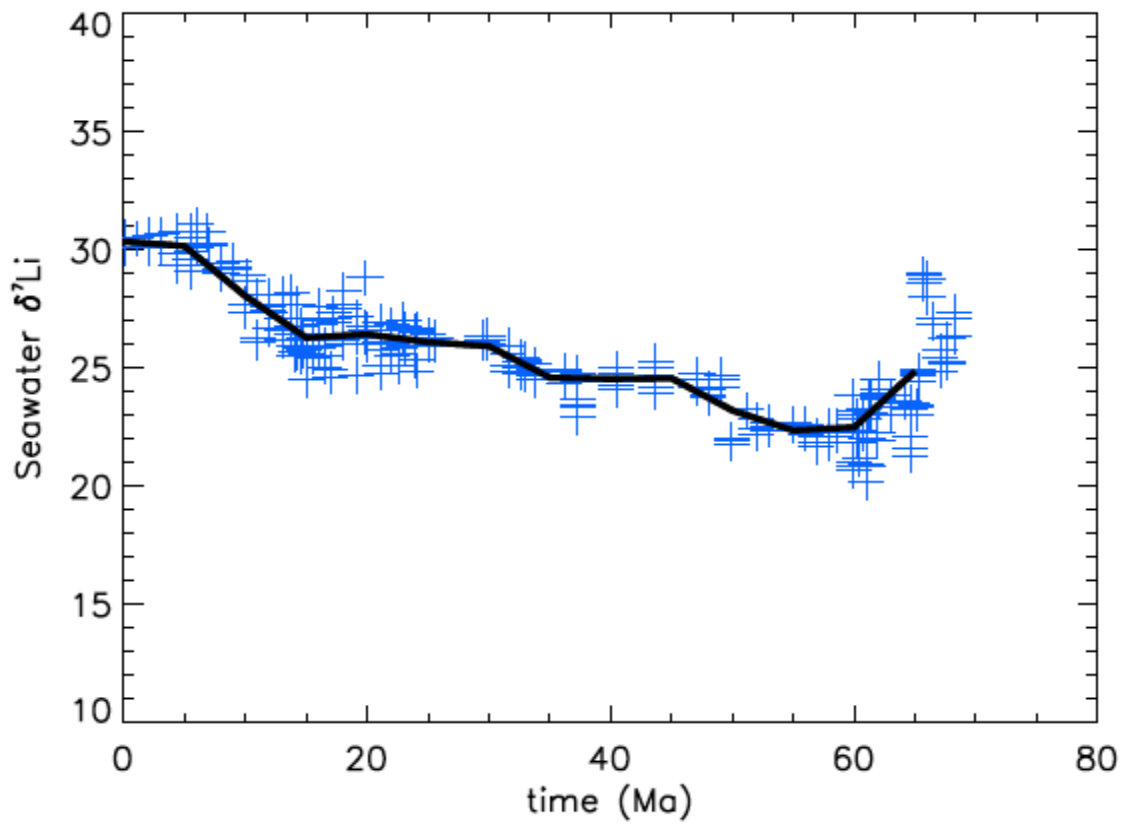
685 **Table 2:** Parameters used the model. Δ_{oc} and Δ_{land} (Li isotope fractionation during secondary
686 phase formation in the ocean and on land respectively) are chosen from within the published
687 range, such that 1/ the seawater paleo-variation exactly match the 5Myr fit of the Misra and
688 Froelich (2012) foraminifera data through the Cenozoic (0-65Ma) (shown in figure 1) and 2/
689 at time t=0 (present day), both $F_{riv}(Li)$ and δ^7Li_{riv} values must be within the published range
690 (see text for references).

	Published values	Model values
$F_{riv}(Li)$	4-12.10 ⁹ mol/yr	Free (see figures)
$F_{hyd}(Li)$	2-145.10 ⁹ mol/yr	5.10 ⁹ mol/yr
δ^7Li_{hyd}	8.5±1‰	8
δ^7Li_{UCC}	1.7±2‰	1.7
δ^7Li_{riv}	23±2‰	Fixed at 23‰ / linear / free (see figures)
Δ_{oc}	10-25‰	14‰
Δ_{land}	10-25‰	23‰
$Li/C_{hyd} = 1/k_2$		6.67.10 ⁻⁴
$(Li/(Ca+Mg))_{UCC} = k_1$		7.5.10 ⁻³

691
692
693
694
695
696
697
698

698
699

Figure 1

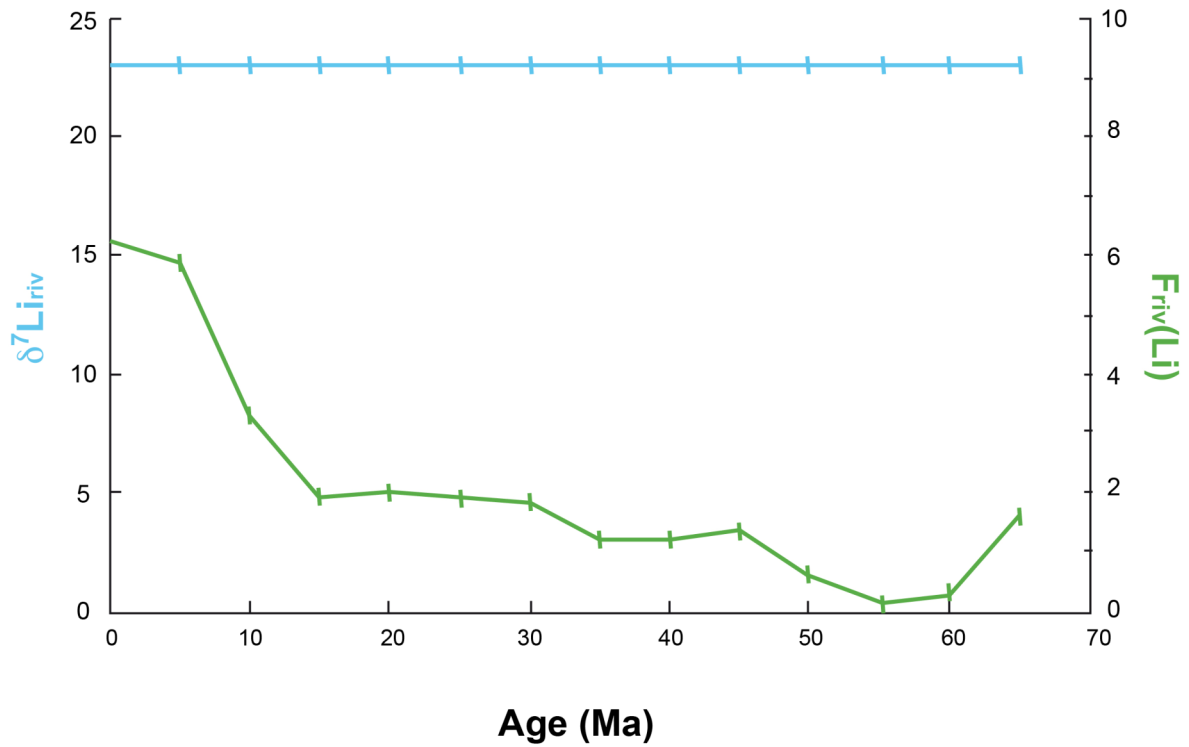


700
701
702
703
704
705
706
707
708

Figure 1: Seawater $\delta^7\text{Li}$ (in ‰) as a function of time (blue symbols), modified from Misra & Froelich (2012), assuming that marine foraminifera and carbonates reflect seawater composition. The black line shows a 5Myr moving average of the data. All model simulations performed in this study are forced to exactly fit this line.

708
709

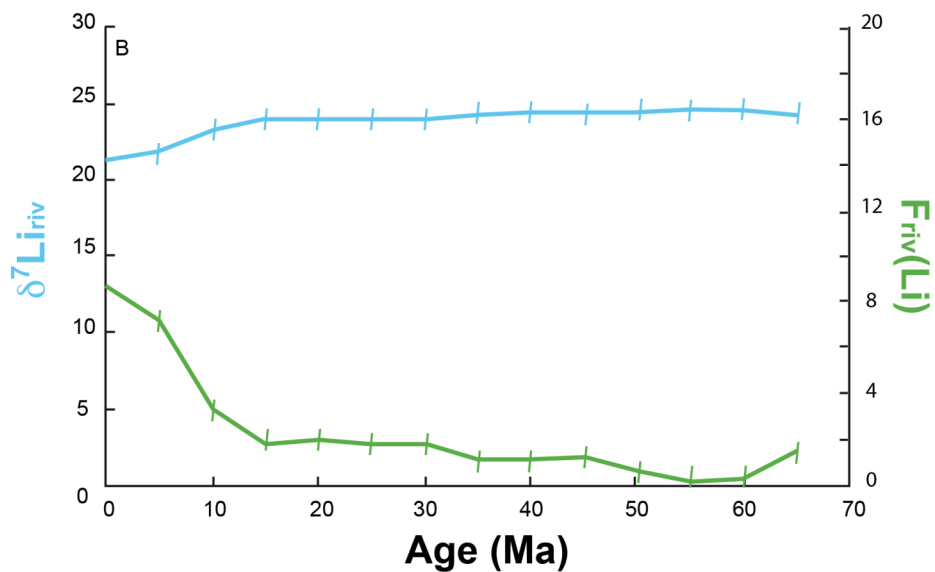
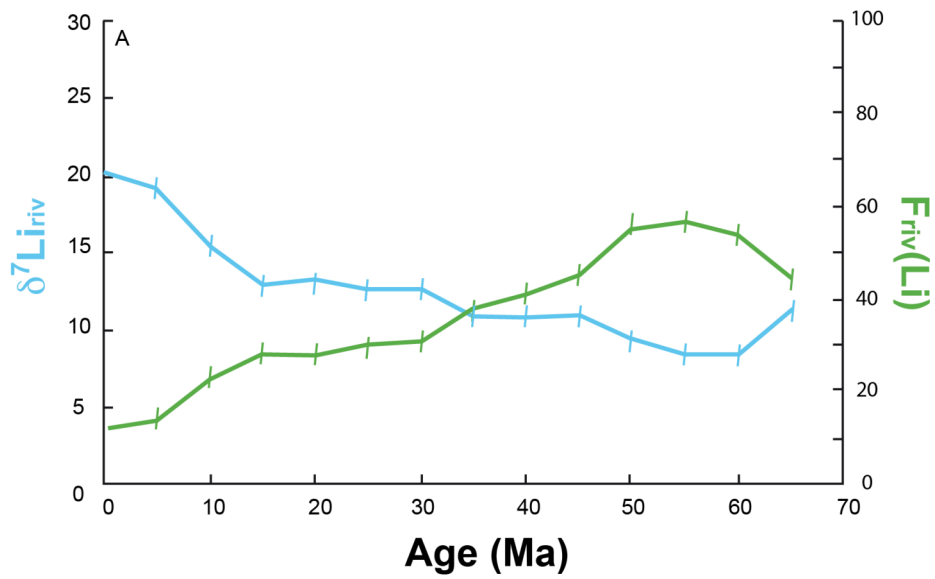
Figure 2



710
711
712
713
714
715
716
717
718

Figure 2: Simulation assuming constant $\delta^7\text{Li}_{\text{riv}}$ (in blue) as a function of time. As shown here, the seawater $\delta^7\text{Li}$ record presented in figure 1 can still be fitted if the flux of river Li (F_{riv} in 10^9 mol/yr, in green) increased significantly during the same period of time. This example demonstrates the lack of constraints on the steady-state model if only the equation for Li is considered. In addition this example shows that river $\delta^7\text{Li}$ can display temporal variations that are significantly different from the ocean $\delta^7\text{Li}$ record.

Figure 3



719

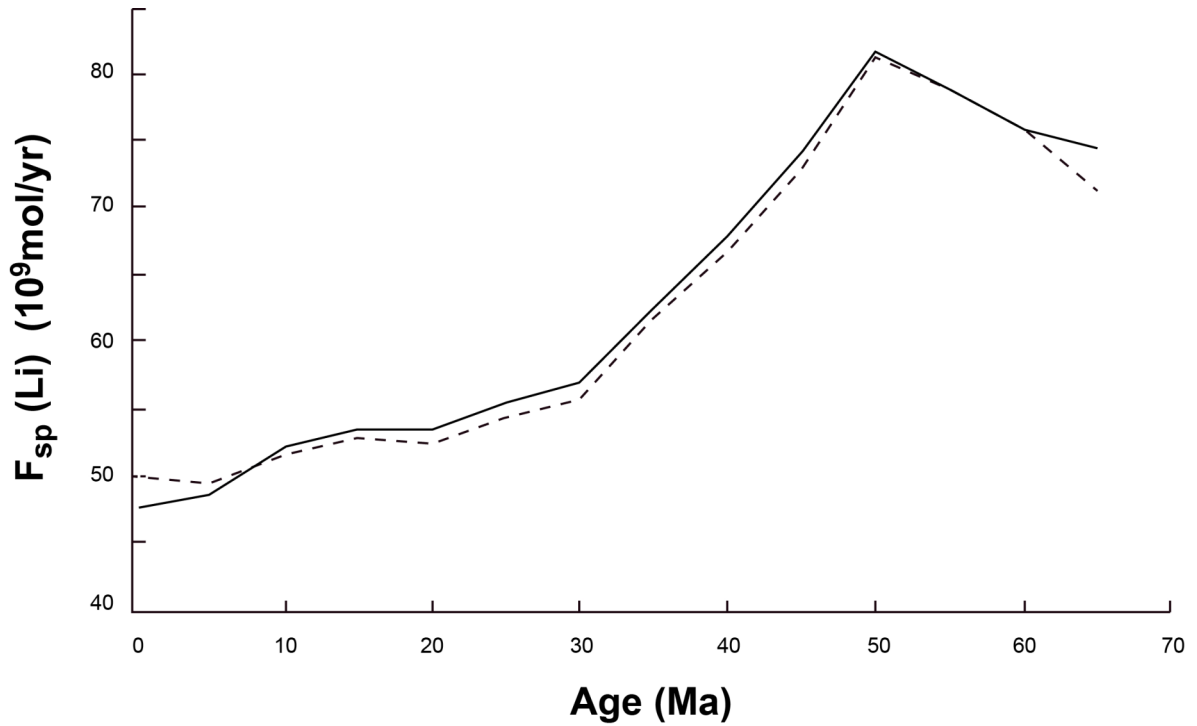
720 **Figure 3A&B:** The two solutions of the model described in the text that can both explain the
 721 seawater record (see equations 3-12, and Table 2) F_{riv} is in 10^9 mol/yr (in green). **A/** this
 722 solution is consistent with calculations performed by Misra & Froelich (2012) since low δ^7Li
 723 values are found for 60Ma rivers and then increased as a function of time (in blue) **B/** a
 724 second solution is also possible, using exactly the same set of parameters. In this case, river
 725 δ^7Li has decreased as a function of time while the Li river flux has increased.

726

727

727
728

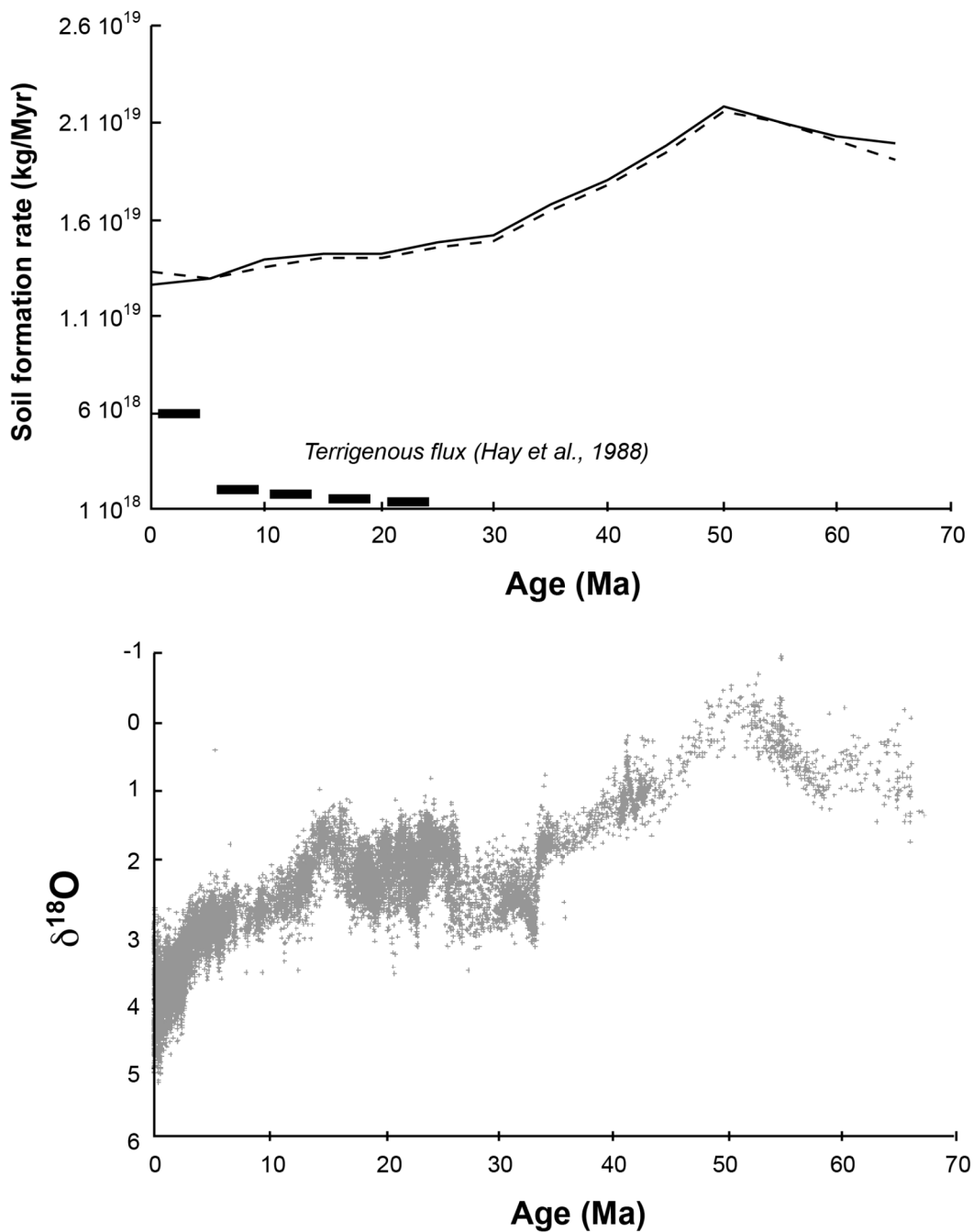
Figure 4



729
730
731
732
733
734
735
736
737
738
739

Figure 4: Flux of lithium incorporated into continental secondary phases as a function of time (F_{sp} , see equation 6), following solution #2 of the modeling (shown in Figure 3B). Comparison is made using a linear evolution for river $\delta^7\text{Li}$ as a function of time, from 15‰ (at 65Ma) to 23‰ (present-day) (dashed line).

Figure 5



740

741 **Figure 5:** A/ Evolution of soil formation rate as a function of time deduced from the
 742 modeling of Li data and assuming that most secondary phases are formed in soils (see text for
 743 more details). A published estimation of evolution of terrigenous flux is shown for
 744 comparison (same unit) B/ Variation of $\delta^{18}\text{O}$ of benthic foraminifera as a function of time
 745 (compilation from Zachos et al., 2001).

746